35th Annual International Conference of the IEEE EMBS
Osaka, Japan, 3 - 7 July, 2013

Combination of intra-operative freehand SPECT imaging with MR images for guidance and navigation

Philipp Matthies[1], Aslı Okur[1], Thomas Wendler[2], Nassir Navab[1] and Michael Friebe[1,3]

Abstract— **Nowadays for clinical applications such as sentinel lymph node biopsy in breast or prostate cancer, only pre-operative image data is used for navigation, i.e. CT, SPECT/CT or PET/CT. Freehand SPECT and freehand PET provide intra-operative functional imaging techniques that can be complemented with pre- and intra-operative MR imaging to allow for better planning, navigation and guidance. In this paper we propose a method to enable navigation based on pre- or intra-operatively acquired MR images. A fully MR compatible phantom and a dedicated MR compatible optical tracking target with MR markers is built for this study. PET/MR, SPECT/CT and freehand SPECT scans of the phantom are performed. Registration is done using point based registration of the known marker and target geometries and a ground truth is obtained from a SPECT/CT and an MR image that are directly registered. The RMS errors was 0.31mm for the ground truth and 3.29mm when using segmentation of the MR markers and their spatial relationship with the optical tracking spheres of the dedicated target. Thus, the freehand SPECT can be registered easily by this approach without the need of any additional CT scans and therefore without any additional radiation dose for the patient. This enables intra-operative fusion of the pre- or intra-operatively acquired MR data, which could provide valuable additional information for intra-operative applications such as guidance based on accurate anatomy or verifying exact tumor location in combination with detailed morphological patient data.**

I. INTRODUCTION

intra-operative imaging is a large field of scientific interest since pre-operative imaging can only be used during surgery in a limited manner applying registration. In most cases, this procedure only provides little additional information due to the deformations and physiological changes between the acquisition time and the actual surgery.

Freehand SPECT enables 3D nuclear imaging of radioactively marked tissue inside the operating room and subsequent navigation to the tissue and verification of the surgical result [1]. In the ideal case for radioguided surgery, the surrounding tissue and organs accumulate much less radioactivity than the targeted anatomical structures and therefore they do not have a major effect on the resulting 3D freehand SPECT images. Thus, the surgeon can easily identify and locate the radioactive hotspots using the 3D navigation provided by the system. Until now, Freehand SPECT has been used mainly on sentinel lymph node biopsy (SLNB) procedures in breast [2], head and neck [3], vulva, penis, cervix, and prostate cancer and melanoma [4].

A combination of different modalities can increase the success of planning, detection and navigation to the structures of interest [5]. Hybrid, intra-operative imaging modalities can provide valuable additional information for the surgeon [6]. For several applications it could be beneficial to complement the intra-operative nuclear functional imaging with pre- or intra-operatively acquired MR images [7], e.g. tumor resection (radical prostatectomy) in medium and big prostate cancer [8], [9]. Recently it has been shown that fusion of PET/CT and MR images for the localization of prostate cancer is superior to each of the individual modalities alone [10].

Prostate cancer is the most diagnosed and second most cause of death by cancer among men in the USA [11]. When having progressed into the regional pelvic lymph nodes it is called lymph-node positive prostate cancer (clinical stage $N1$). Small prostate cancers have a probability of approximately zero of being $N1$ and only the prostate gland with the tumor is resected, whereas medium size prostate cancers are likely to have progressed into the local lymph nodes and the patients are treated with radical prostatectomy combined with SLNB. A SPECT/CT is only done in $\approx 2\%$ of the cases, in the remaining cases the surgeon cuts by only looking at the anatomy. In big tumors the probability for $N1$ is almost 100% and therefore prostate gland (including tumor) and nodes are resected. To find the suspicious nodes, in a few hospitals a ^{11}C-Choline or a ^{18}F-Choline PET/CT or PET/MR is done.

Nowadays for this clinical application only pre-operative image data is used for navigation, i.e. CT, SPECT/CT or PET/CT. The requirements for intra-operative navigation and imaging in prostate cancer comprise an MR image plus an additional intra-operative functional image. For SLNB a freehand SPECT image can be acquired intra-operatively. For finding metastatic lymph nodes in big tumor cases, an acquisition of an intra-operative freehand PET image can be considered in the future as introduced by Shakir et al. [12] for head and neck cancer.

In this paper we propose a method to enable navigation based on pre- or intra-operatively acquired MR images. A fully MR compatible phantom and optical tracking target with MR markers are build for this study. After preparation with proper radioactive tracers, PET/MR, SPECT/CT and freehand SPECT scans of the phantom are performed. Registration is done using point based registration of the known

[1]P. Matthies, A. Okur and N. Navab are with the Faculty of Computer Science, Chair for Computer Aided Medical Procedures, Technische Universität München, Germany, {matthies,okur,navab} at in.tum.de;

[2]T. Wendler is with SurgicEye GmbH, München, Germany, wendler at surgiceye.com

[3]M. Friebe is with the TUM Institute for Advanced Study and Chair for Computer Aided Medical Procedures, Technische Universität München, Germany, friebe at in.tum.de

978-1-4577-0216-7/13/$26.00 ©2013 IEEE

marker and target geometries. Furthermore, the ground truth is obtained from a SPECT/CT and an MR image that are directly registered by segmenting the spheres of the phantom which are clearly visible in both modalities. The RMS errors are calculated for both of the approaches.

II. MATERIALS & METHODS

A phantom suited for SPECT/CT, PET/MR and freehand SPECT imaging was built and scans with the mentioned modalities were performed. The optical tracking target necessary for freehand SPECT was correlated with the adjacent MR markers using the CT data. Finally image fusion is done using point based registration.

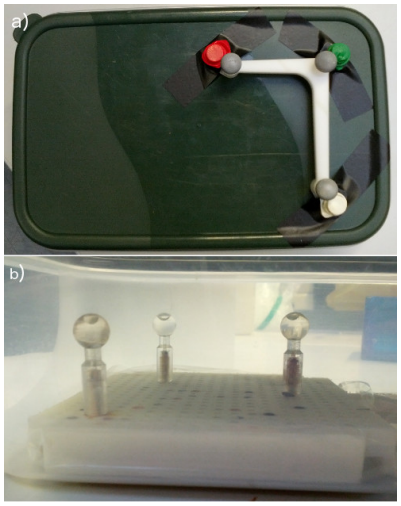

Fig. 1. (a) The MR compatible reference target for the optical tracking combined with MR markers attached close to the retroreflective spheres. (b) The hollow spheres inside the phantom are filled with [^{18}F]FDG for the PET/MR and ^{99m}Tc for the SPECT/CT and freehand SPECT scans.

A. Phantom

A phantom was made for this research, similar to commonly used phantoms for nuclear functional imaging applications [13], but with the major difference of being 100% MR compatible. Fig. 1 shows the top (a) and side (b) views on the phantom. The optical tracking target with the L-shape (6.7cm by 5.0cm) and the three retroreflective spheres is expanded by three MR markers close to the respective spheres. In this early prototype, small plastic boxes were glued onto the optical tracking target (red, green and white cylinders) and filled with an MR contrast agent (sodium iodide solution mixed with gadolinium) as the L-shaped part and the spheres are made of plastic and therefore not visible in MR images. The metal pins holding the retrospective spheres were replaced with wooden ones resulting in an MR compatible and clearly identifiable target.

A plastic base plate inside the phantom holds the hollow spheres filled with radioactive solution with wooden pins instead of metal screws (Fig. 1 (b)). The hollow spheres are filled with [^{18}F]FDG for PET/CT acquisition and with ^{99m}Tc for the SPECT/CT and the freehand SPECT acquisitions. The whole box can be filled with saline solution to represent human tissue in CT and MR images.

B. SPECT/CT

A SPECT/CT (Siemens Symbia T6) of the phantom was acquired with a total activity of 9.5MBq of ^{99m}Tc distributed over the three spheres (3.4MBq, 3.2MBq and 2.9MBq, respectively). CT resolution was 0.35mm in x- and y-direction and 0.8mm in z-direction (patient table axis). SPECT parameter were 3D OSEM iterative solver with 8 iterations and 15 subsets, Gaussian filtering with 8.4mm, an energy windows between 129.5 and 150.5keV and attenuation correction based on CT activated. Fig. 2 shows the fused SPECT/CT image rendered in 3D. In the CT image the MR marker, the spheres for optical tracking and the spheres filled with ^{99m}Tc are visible, the latter covered by the SPECT image information.

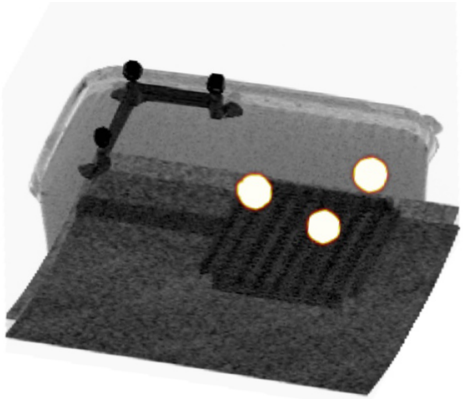

Fig. 2. Fused SPECT/CT image shown in a maximum intensity projection rendering. The water-filled phantom with the optical tracking target in the upper left and the three radioactively filled spheres in the lower right part is visible. The lower part of the image is the patient table of the scanner.

C. PET/MR

We used a Siemens Biograph mMR which uses a 3T constant magnetic field to acquire PET/MR images of the phantom. The hollow spheres were filled with 10.0MBq, 11.2MBq and 9.8MBq of [^{18}F]FDG, respectively, and box was filled with saline solution. For the MR images we selected a 3D VIBE sequence for high resolution (TA 1:22min, TR 4.07ms, TE 1.6ms) with an isotropic voxel size of 0.8mm and a flip angle of 5°. The Biograph mMR PET system consists of APD detectors and we chose an acquisition time of 15min for sufficient visual image quality. The final images were reconstructed using an OSEM 3D iterative solver with 3 iterations and 21 subsets filtered with a 4mm Gaussian filter for artifact reduction and smoothness. The PET data looks very similar to the SPECT data and is not shown here.

D. Freehand SPECT

A Freehand SPECT reconstruction of the radiation distribution in the phantom is generated using a *declipseSPECT* cart system (SurgicEye, Germany), which includes a *Gamma-Probe System* gamma detector with a 60° collimator

(Crystal Photonics, Germany) for radiation detection and a *Polaris Vicra* infrared optical tracking system (Northern Digital, Canada) for spatial positioning. The operator scanned the volume of interest (VOI) in a freehand fashion for 192 seconds covering multiple angles on 4 sides of the plastic box (cp. Fig. 3 (a)) which resulted in 4000 measurements. The reconstruction is performed using MLEM with 20 iterations, the image is filtered (6mm Gaussian) and thresholding for better visualization is applied.

For this scan the three spheres (cp. Fig. 1 (b)) in the phantom were filled with ^{99m}Tc (2.7MBq (1), 2.5MBq (2) and 2.3MBq (3), respectively).

The reconstructed volume can be augmented using the integrated camera (Fig. 3 (a)). It also can be visualized in a virtual reality view such that the image is seen from the tip of the probe. This mode allows intuitive navigation inside the volume and concrete depth measurements to segmented hotspots in the reconstructed image (Fig. 3 (b)).

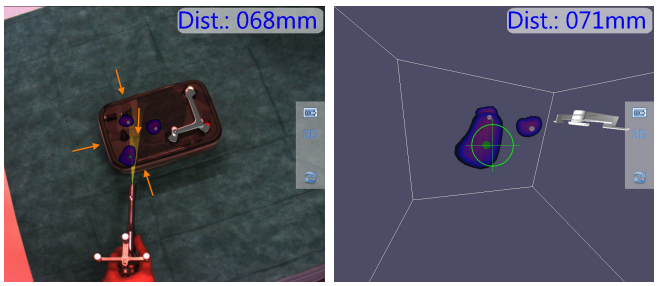

Fig. 3. Freehand SPECT visualization in two different modes: (a) as seen from the camera using augmented reality, (b) as seen from the probe tip in virtual reality mode. The arrows in (a) show the 4 scanning planes, 3 from the sides and one from top.

E. Point Based Registration

For the registration between the SPECT/CT and the MR image data we used two approaches, one to obtain a ground truth based on prior knowledge and one that can be used later in applications without knowing corresponding points. The different approaches are explained in Fig. 4. For the ground truth the three radioactively filled spheres were manually segmented in the SPECT/CT image and in the MR image, respectively. Using a point based registration [14], a transformation between these two coordinate systems ${}^{mr}\mathbf{T}_{ct}$ and its RMS error are calculated. This reveals a direct relation between a point in the MR image ($\vec{x}_{mr}$) and a corresponding point the SPECT/CT image ($\vec{x}_{ct}$):

$$\vec{x}_{mr} = {}^{mr}\mathbf{T}_{ct} \cdot \vec{x}_{ct} \tag{1}$$

The second approach, which is usable without prior knowledge of corresponding points, involves three different coordinate transformations:

$$\vec{x}_{mr} = {}^{mr}\mathbf{T}_{marker} \cdot {}^{marker}\mathbf{T}_{target} \cdot {}^{target}\mathbf{T}_{ct} \cdot \vec{x}_{ct} \tag{2}$$

${}^{target}\mathbf{T}_{ct}$ transforms from the CT coordinate system to the one of the optical tracking target and is obtained by segmentation of the optical tracking spheres in the CT dataset and a subsequent translation and rotation. ${}^{mr}\mathbf{T}_{marker}$ transforms from the coordinate system of the MR markers to the one of the MR origin and is obtained in the same way as ${}^{target}\mathbf{T}_{ct}$, only that the MR markers are segmented in the MR dataset this time. ${}^{marker}\mathbf{T}_{target}$ is the transformation between the coordinate system of the optical tracking target and the one of the MR markers (cp. Fig. 4, top). It is solely dependent on the geometry of the combined optical and MR tracking target. For this study this transformation is obtained using the CT image.

III. EVALUATION & RESULTS

To evaluate the accuracy of the registered freehand SPECT and MR images, we registered the MR directly with the SPECT image by manually selecting the center of the spheres in both datasets and calculating the point based registration. This serves as a ground truth for the registration. The RMS error of this coordinate transformation was 0.31mm. Fig. 5 shows this result as a 3D visualization of the SPECT scan overlaid with the respective MR image using OsiriX software. Clearly the three ^{99m}Tc filled spheres are visible and below them barely recognizable the inverse shapes of the wooden holders and the plastic grid. The three cylinders above the phantom on the left are the contrast enhanced MR markers (using Gadolinium) and the "noise" above the phantom is mostly drops of water on the ceiling of the inner side of the phantom.

The registration using segmentation of the MR markers, their spatial relationships with the optical tracking spheres and segmentation of these spheres in the respective SPECT/CT image, as described in the section above, yielded a RMS error of 3.29mm.

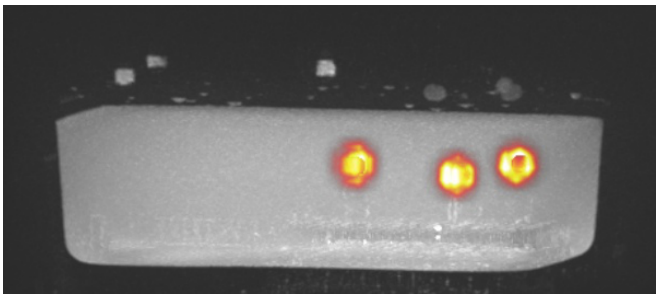

Fig. 5. 3D visualization of the SPECT scan of the phantom registered and overlaid with the respective MR image. Clearly the three ^{99m}Tc filled spheres and the three contrast enhanced cylinders above the phantom on the left are visible. The "noise" above the phantom is mostly drops of water on the ceiling of the inner side of the phantom.

IV. CONCLUSIONS

For quantitative evaluation of the approach we used SPECT/CT instead of freehand SPECT since it provides a much higher resolution and accuracy and is the state-of-the-art for the diagnosis. However, since it cannot be used inside the operating room, the actual usage in a clinical setting would be the combination of pre- or intra-operative MR data and intra-operative freehand SPECT.

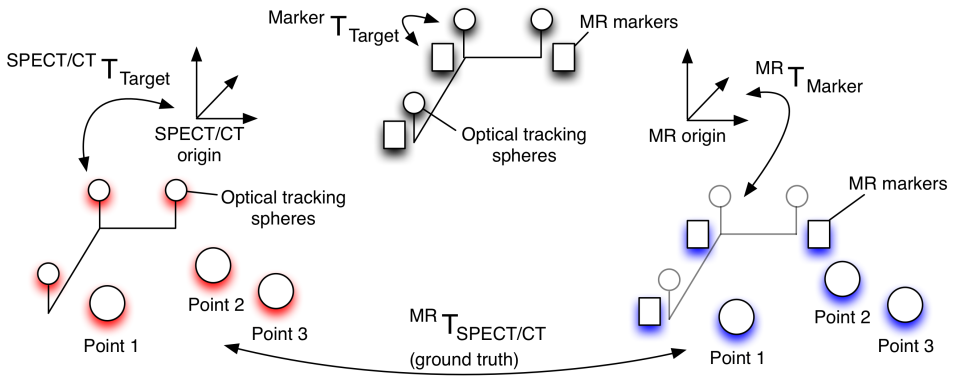

Fig. 4. For the ground truth the three radioactively filled spheres (points 1-3 on the left) were manually segmented in the SPECT/CT image and in the MR image (right), respectively. A direct transformation between these two coordinate systems is calculated. The second approach, which is usable without prior knowledge of corresponding points, involves three different coordinate transformations illustrated above: ${}^{target}\mathbf{T}_{ct}$ transforms from the SPECT/CT or fhSPECT coordinate system to the one of the optical tracking target and is obtained by segmentation of the optical tracking spheres in the CT dataset (left). Analogously ${}^{mr}\mathbf{T}_{marker}$ is obtained for the MR data (right). ${}^{marker}\mathbf{T}_{target}$ transforms between the optical tracking spheres and the MR markers (top). It is solely dependent on the geometry of the combined optical and MR tracking target.

Eventhough the direct calculation of the transformation from SPECT/CT to MR coordinate system serving as the ground truth provides a much better registration, the registration error that we achieved by using a both MR and freehand SPECT compatible reference target is considerably small (<5mm). The exact geometry of the tracking target and the transformation ${}^{marker}\mathbf{T}_{target}$ can be obtained either by a CT scan or directly by construction measures if produced by rapid prototyping. Thus, the freehand SPECT can be registered easily without the need of any additional CT scans inbetween and therefore without any additional radiation dose for the patient. This enables intra-operative fusion of the the pre- or intra-operatively acquired MR data, which could provide valuable additional information for intra-operative applications such as verifying exact tumor location in combination with detailed morphological patient data.

Future works could include in-depth analysis and experiments using pre- and intra-operative data from patients as well as implementation of better registration methods taking into account the deformations during surgery (e.g. geometrical shape in the neighborhood of the target structures).

ACKNOWLEDGMENT

This research was partially funded by the SFB 824 of the Deutsche Forschungsgesellschaft (DFG) and the TUM Institute for Advanced Study, funded by the German Excellence Initiative.

REFERENCES

[1] T. Wendler, K. Herrmann, A. Schnelzer, T. Lasser, J. Traub, O. Kutter, A. Ehlerding, K. Scheidhauer, T. Schuster, M. Kiechle, M. Schwaiger, N. Navab, S. I. Ziegler, and A. K. Buck, "First demonstration of 3-D lymphatic mapping in breast cancer using freehand SPECT," *Eur J Nucl Med Mol Imaging*, vol. 37, no. 8, pp. 1452–1461, Aug. 2010.

[2] A. Schnelzer, A. Ehlerding, C. Blümel, A. Okur, K. Scheidhauer, S. Paepke, and M. Kiechle, "Showcase of intraoperative 3D imaging of the sentinel lymph node in a breast cancer patient using the new freehand SPECT technology," *Breast Care*, vol. 7, no. 6, pp. 484–486, 2012.

[3] D. A. Heuveling, K. H. Karagozoglu, A. van Schie, S. van Weert, A. van Lingen, and R. de Bree, "Sentinel node biopsy using 3D lymphatic mapping by freehand SPECT in early stage oral cancer: a new technique," *Clinical Otolaryngology*, vol. 37, no. 1, pp. 89–90, Feb. 2012.

[4] S. Naji, A. Tadros, J. Traub, and C. Healy, "Case report: Improving the speed and accuracy of melanoma sentinel node biopsy with 3D intraoperative imaging," *Journal of Plastic, Reconstructive & Aesthetic Surgery*, vol. 64, no. 12, pp. 1712–1715, Dec. 2011.

[5] O. Brouwer, T. Buckle, A. Bunschoten, J. Kuil, A. Vahrmeijer, T. Wendler, R. Valdes-Olmos, H. van der Poel, and F. Van Leeuwen, "SPECT/CT navigation as a means to improve the accuracy of radio- and fluorescence guided surgery," *J Nucl Med Meeting Abstracts*, vol. 53, no. 1 Meeting Abstracts, p. 1158, 2012.

[6] T. Wendler, T. Lasser, S. I. Ziegler, and K. Scheidhauer, "Freehand SPECT/US: new approach for intraoperative hybrid imaging of sentinel nodes," in *Proceedings of the ISNS 2010*. Yokohama, Japan: ISNS, Nov. 2010.

[7] G. Krombach, A. Buecker, J. Pfeffer, C. Hohl, J. Temur, M. Friebe, S. Kinzel, and R. Guenther, "Development of a catheter for MRI-guided intramyocardial injection," in *ISMRM-ESMRMB*, 2007.

[8] J. Tokuda, G. S. Fischer, S. P. Dimaio, D. G. Gobbi, C. Csoma, P. W. Mewes, G. Fichtinger, C. M. Tempany, and N. Hata, "Integrated navigation and control software system for MRI-guided robotic prostate interventions," *Comput Med Imaging Graph*, vol. 34, no. 1, pp. 3–8, Jan 2009.

[9] P. Puech, A. S. Iancu, B. Renard, A. Villers, and L. Lemaitre, "Detecting prostate cancer with MRI - why and how," *Diagnostic and Interventional Imaging*, vol. 93, no. 4, pp. 268 – 278, 2012.

[10] I. Jambor, R. Borra, J. Kemppainen, V. LepomÃki, R. Parkkola, K. Dean, K. Alanen, E. Arponen, M. Nurmi, H. J. Aronen, and H. Minn, "Improved detection of localized prostate cancer using co-registered MRI and 11C-acetate PET/CT," *European Journal of Radiology*, vol. 81, no. 11, pp. 2966 – 2972, 2012.

[11] A. Jemal, R. Siegel, E. Ward, T. Murray, J. Xu, and M. J. Thun, "Cancer statistics, 2007," *CA: A Cancer Journal for Clinicians*, vol. 57, no. 1, pp. 43–66, 2007.

[12] D. Shakir, A. Okur, A. Hartl, P. Matthies, S. Ziegler, M. Essler, T. Lasser, and N. Navab, "Towards Intra-operative PET for Head and Neck Cancer: Lymph Node Localization Using High-Energy Probes," in *Proceedings of MICCAI*. Springer, 2012, vol. 7510, pp. 430–437.

[13] T. Wendler, A. Hartl, T. Lasser, J. Traub, F. Daghighian, S. Ziegler, and N. Navab, "Towards intra-operative 3d nuclear imaging: Reconstruction of 3d radioactive distributions using tracked gamma probes," in *Proceedings of MICCAI*. Springer, 2007, vol. 4792, pp. 909–917.

[14] S. Umeyama, "Least-squares estimation of transformation parameters between two point patterns," *Pattern Analysis and Machine Intelligence, IEEE Transactions on*, vol. 13, no. 4, pp. 376 –380, apr 1991.